Research Letter **DOI:** 10.15541/jim20240345

Na and O Co-doped Carbon Nitride for Efficient Photocatalytic Hydrogen Evolution

CHEN Libo[1], SHENG Ying[1], WU Ming[1], SONG Jiling[2], JIAN Jian[1], SONG Erhong[3]

(1. School of Chemistry and Chemical Engineering, Hunan University of Science and Technology, Xiangtan 411201, China;
2. National Engineering Research Center for Compounding and Modification of Polymer Materials, Guiyang 550014, China;
3. Shanghai Institute of Ceramics, Chinese Academy of Sciences, Shanghai 200050, China)

Abstract: Elemental doping is an effective strategy for tuning the band structure of graphite carbon nitride (CN) to enhance its photocatalytic performance. In this study, sodium (Na) and oxygen (O) co-doped carbon nitride (Na/O-CN_x, x=1.0, 2.0, 3.0, 4.0) was synthesized *via* solid-phase reaction of sodium citrate (NaCA) and pure CN powder in the Teflon-sealed autoclave under air conditions at 180 ℃. Surface area of Na/O-$CN_{3.0}$ is measured to be 18.8 m^2/g, increasing by 60.7% compared to that of pure CN (11.7 m^2/g). Bandgap energy of Na/O-$CN_{3.0}$ is determined to be 2.68 eV, marginally lower than that of pure CN (2.70 eV), thereby enhancing its capacity for sunlight absorption. Meanwhile, the incorporation of Na and O atoms into Na/O-CN_x is found to effectively reduce recombination rates of photogenerated electron-hole pairs. As a result, Na/O-CN_x samples exhibit markedly enhanced photocatalytic hydrogen evolution activity under visible light irradiation. Notably, the optimal Na/O-$CN_{3.0}$ sample achieves a photocatalytic hydrogen production rate of 103.2 $\mu mol\cdot g^{-1}\cdot h^{-1}$, which is 8.2 times greater than that of pure CN (11.2 $\mu mol\cdot g^{-1}\cdot h^{-1}$). Furthermore, a series of Na/O-CN_x-yO_2 (y=0, 20%, 40%, 60%, 80%, 100%) samples were prepared by modulating the oxygen content within reaction atmosphere. The catalytic performance evaluations reveal that the incorporation of both Na and O atoms in Na/O-$CN_{3.0}$ enhances photocatalytic activity. This study also introduces novel methodologies for synthesis of metal atom-doped CN materials at lower temperature, highlighting the synergistic effect of Na and O atoms in photocatalytic hydrogen production of Na/O-CN_x samples.

Key words: Na and O co-doped carbon nitride; synergistic effect; visible light; photocatalytic hydrogen evolution

The global energy shortage and environmental pollution are two major challenges facing humanity[1-6]. To address these issues, various clean energy sources with environmentally friendly characteristics are being explored[7]. Among them, hydrogen is regarded as one of the most promising clean energy sources[8-15]. However, industrial hydrogen production currently relies heavily on fossil resources such as oil, natural gas, and coal. Therefore, the development of green hydrogen production technologies is both necessary and challenging[16-17]. Among various methods, photocatalytic hydrogen production has emerged as a promising solution[18-24], and the key to its industrial application lies in identifying suitable semiconductors that can achieve highly efficient hydrogen evolution rates.

Metal-free graphite carbon nitride (g-C_3N_4) has garnered significant attention in the field of photocatalysis since its photocatalytic hydrogen evolution activity was first discovered in 2009[25]. g-C_3N_4 possesses a suitable band structure for water splitting under visible light irradiation, along with excellent physical and chemical stability[26-27]. However, conventional g-C_3N_4 faces limitations in industrial hydrogen production due to its low efficiency in utilizing photogenerated electron-hole

Received date: 2024-07-20; **Revised date:** 2024-10-15; **Published online:** 2024-10-28
Foundation item: National Natural Science Foundation of China (21806023); Natural Science Foundation of Hunan Province (2021JJ40199); Education Department Foundation of Hunan Province (20C0813); Hunan University of Science and Technology Fundamental Research Funds; Postgraduate Scientific Research Innovation Project of Hunan Province (CX20240877)
Biography: CHEN Libo (2000–), male, Master candidate. E-mail: 1871066627@qq.com
陈莉波(2000–), 男, 硕士研究生. E-mail: 1871066627@qq.com
Corresponding author: WU Ming, associate professor. E-mail: wuming10@mails.jlu.edu.cn;
SONG Erhong, associate professor. E-mail: ehsong@mail.sic.ac.cn
伍 明, 副教授. E-mail: wuming10@mails.jlu.edu.cn; 宋二红, 副研究员. E-mail: ehsong@mail.sic.ac.cn

pairs[28-30]. To overcome this problem, alkali metal doping has been identified as an effective approach. For instance, Wu *et al*.[31] demonstrated enhanced photocatalytic hydrogen evolution in g-C_3N_4 through K doping. Zhu *et al*.[32] improved the charge carrier separation efficiency of g-C_3N_4 by incorporating Na^+ into its framework. Zhao *et al*.[33] enhanced the photocatalytic activity of porous graphitic carbon nitride nanorods by adding functional Na^+. Han *et al*.[34] improved photocatalytic hydrogen evolution in Na-doped g-C_3N_4 using a NH_4Cl-assisted method. Similarly, Dou *et al*.[35] developed willow-shaped g-C_3N_4 with sodium doping, achieving enhanced photocatalytic performance under visible light. There is a consensus that Na doping is an effective strategy for improving the photocatalytic activity of g-C_3N_4. Meanwhile, O doping has also been reported as another promising approach[36-37]. Hence, designing Na and O co-doped g-C_3N_4 is expected to further enhance photocatalytic activity. Ren *et al*.[38] synthesized Na and O co-doped g-C_3N_4 for H_2O_2 production, indirectly supporting this hypothesis. However, the potential of Na and O co-doped g-C_3N_4 in photocatalytic hydrogen production remains unclear, particularly regarding the synergistic effects between Na and O atoms, which requires further experimental exploration.

In this work, carbon nitride co-doped with Na and O (Na/O-CN_x) was synthesized using NaCA as sodium source. The enhanced photocatalytic activities of Na/O-CN_x samples were thoroughly analyzed through structural, compositional, and optical performance characterizations. Additionally, the synergistic effects in Na/O-CN_x were elucidated through comparative studies of pure CN, Na/O-CN_x, and Na/O-$CN_{3.0}$-yO_2 samples by using carefully planned experiments.

1 Experimental

1.1 Chemicals

Melamine ($C_3H_6N_6$, Aladdin Chemistry, ⩾ 99%), sodium citrate tribasic dihydrate ($C_6H_5Na_3O_7·2H_2O$, Aladdin Chemistry, ⩾ 99%), triethanolamine ($C_6H_{15}NO_3$, Sinopharm Reagent, ⩾ 99%) and chloroplatinic acid hexahydrate ($H_2PtCl_6·6H_2O$, J&K Scientific Co., Ltd., ⩾99.9%) were used without any purification. Deionized water was produced by Unique-R10 with a specific resistance of 18.2 MΩ·cm.

1.2 Preparation of pure CN sample

Pure CN powder was synthesized following a reported method[34, 39]. Melamine (10 g) was heated in a muffle furnace at 550 ℃ for 4 h in static air with a ramp rate of 10 ℃/min. The reaction took place in a covered crucible, and the resulting CN powder was ground using an agate mortar.

1.3 Preparation of Na/O-CN_x and Na/O-$CN_{3.0}$-yO_2 samples

The synthesis process of Na/O-CN_x samples is shown in Fig. 1. Pure CN (1.0 g) was mixed with *x* g (*x*=1.0, 2.0, 3.0, 4.0) of sodium citrate, and the mixture was ground for 10 min using a mortar. The resulting powders were placed in a Teflon-sealed autoclave (25 mL) and heated in the oven at 180 ℃ for 6 h. This synthesis temperature is lower than that used in many other alkali metal-doped carbon nitride processes (Table S1). After cooling to room temperature, the samples were washed with water three times and dried at 50 ℃ for 12 h, yielding Na/O-CN_x samples (*x*=1.0, 2.0, 3.0, 4.0).

Na/O-$CN_{3.0}$-yO_2 samples were prepared using 3.0 g of sodium citrate under varying oxygen contents (*y*=0, 20%,

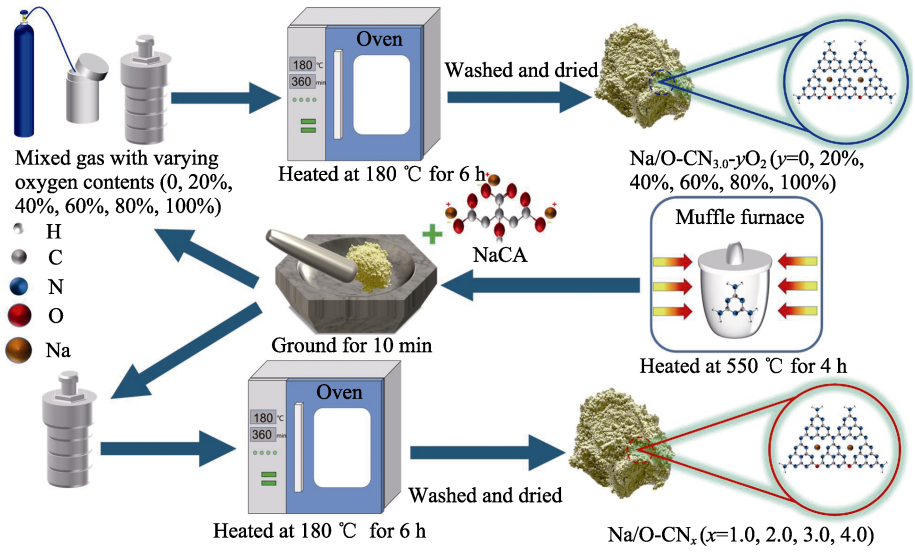

Fig. 1　Synthetic schematic of Na/O-CN_x and Na/O-$CN_{3.0}$-yO_2 samples

40%, 60%, 80%, 100%, in volume) in a mixture of oxygen and nitrogen gases instead of air. The resulting samples were labeled as Na/O-$CN_{3.0}$-0O_2, Na/O-$CN_{3.0}$-20%O_2, Na/O-$CN_{3.0}$-40%O_2, Na/O-$CN_{3.0}$-60%O_2, Na/O-$CN_{3.0}$-80%O_2, and Na/O-$CN_{3.0}$-100%O_2.

1.4 Photocatalytic activity test and materials characterization

Details on the photocatalytic hydrogen evolution test and materials characterization can be found in the supporting materials.

2 Results and discussion

2.1 Morphologies and structures characterization

The structures of the synthesized Na/O-CN_x samples were analyzed *via* X-ray diffractometer (XRD), as shown in Fig. 2(a, b). All peaks of Na/O-CN_x samples align with those of pure CN at 2θ=13.0° and 27.5°[33, 40-41], indicating that the in-plane and interlayer structures of carbon nitride remain intact. However, the peak intensity at 2θ=27.5° of Na/O-CN_x samples increases compared to pure CN, suggesting that Na and O co-doping enhances the crystallinity of Na/O-CN_x[42-44]. Similar phenomena are observed in Na/O-$CN_{3.0}$-$y$$O_2$ samples depicted in Fig. 2(b), indicating that main structures of Na/O-$CN_{3.0}$-$y$$O_2$ remain intact, with only the crystallinity of samples being affected by the doping Na and O atoms. Fourier transform infrared (FT-IR) spectra of samples have also been operated for analyzing their structures, as shown in Fig. 2(c). Na/O-$CN_{3.0}$ and Na/O-$CN_{3.0}$-40%O_2 samples exhibit the same peaks in the range of 807–880 cm^{-1}, corresponding to the out-of-plane bending mode of the triazine ring in carbon nitride[45]. Additionally, Na/O-$CN_{3.0}$ and Na/O-$CN_{3.0}$-40%O_2 samples also show the same absorption peaks in the range of 1200–1700 cm^{-1} compared to pure CN, corresponding to the aromatic C–N heterocycle structures in carbon nitride[46]. In contrast, the peaks in the range of 3100–3400 cm^{-1} for Na/O-CN_x slightly shift compared to pure CN, indicating that the stretching vibrations of –N–H groups in Na/O-CN_x are altered due to Na and O doping[47-49]. Consequently, the electronic structure of Na/O-CN_x is tuned by the synergistic effects of Na and O co-doping[50].

Scanning electron microscope (SEM) images (Fig. 3(a, b)) reveal that Na/O-$CN_{3.0}$ has a block-like structure similar to pure CN with no structural damage after the reaction in the Teflon-sealed autoclave. Transmission electron microscope (TEM) images (Fig. 3(c, d)) confirm that the nanosheet structure of Na/O-$CN_{3.0}$ is also similar to that of pure CN[51]. High-resolution TEM (HRTEM) image (Fig. 3(d)) indicates a lattice spacing of 0.33 nm for Na/O-$CN_{3.0}$, consistent with (002) plane (JCPDS #87-1526)[26, 34, 52]. However, slight structural differences between Na/O-$CN_{3.0}$ and pure CN are evident through Brunauer-Emmett-Teller (BET) analysis (Fig. S1). The surface area of Na/O-$CN_{3.0}$ is 18.8 m^2/g, 60.7% larger than that of pure CN (11.7 m^2/g). This value is even larger than some alkali metal-doped carbon nitrides synthesized at higher temperatures, as indicated in Table S1. Additionally, Na/O-$CN_{3.0}$ exhibits a larger pore volume (0.039 cm^3/g) compared to pure CN (0.023 cm^3/g). These changes in the surface area of Na/O-$CN_{3.0}$ may result from oxidation reactions with O_2 from the air or the solid-phase reaction[53] between pure CN and sodium citrate in the Teflon-sealed autoclave under high temperature and pressure. As a result, Na/O-$CN_{3.0}$ with

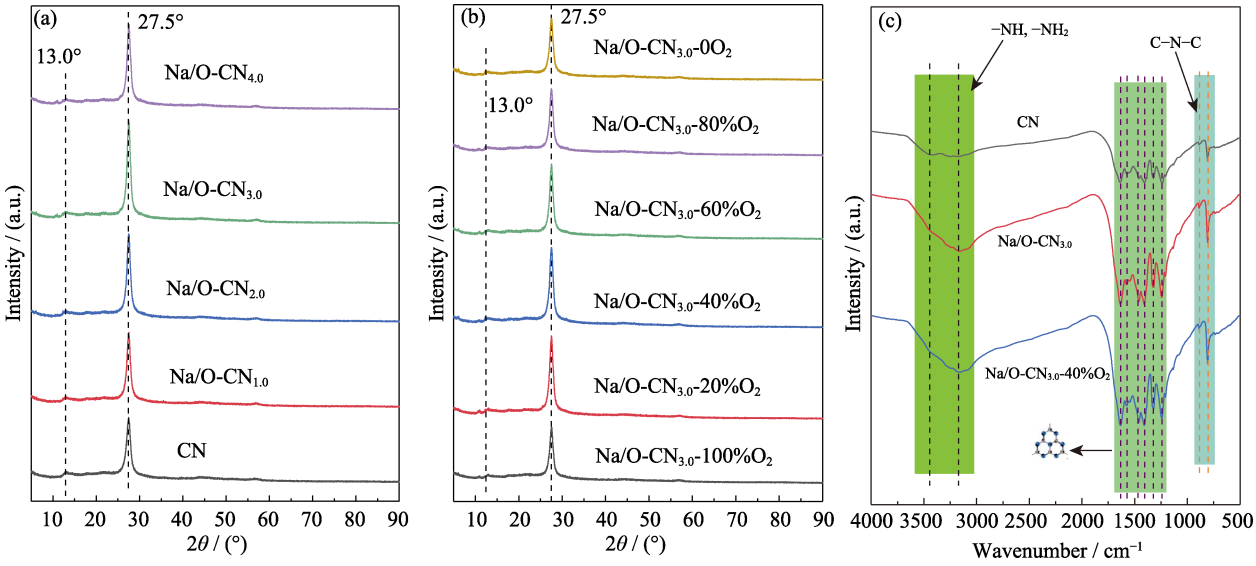

Fig. 2 Structure analyses of samples

(a, b) XRD patterns of (a) pure CN and Na/O-CN_x, and (b) Na/O-$CN_{3.0}$-$y$$O_2$; (c) FT-IR spectra of pure CN, Na/O-$CN_{3.0}$ and Na/O-$CN_{3.0}$-40%O_2

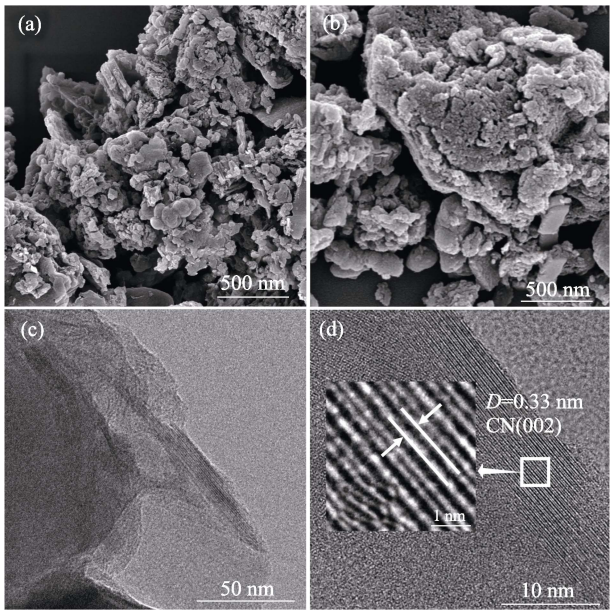

Fig. 3　Morphologies of samples
(a, b) SEM images of (a) pure CN and (b) Na/O-$CN_{3.0}$; (c) TEM and (d) HRTEM images of Na/O-$CN_{3.0}$

increased reactive sites is expected to enhance photocatalytic hydrogen evolution activity.

The chemical compositions of Na/O-$CN_{3.0}$, pure CN, and Na/O-$CN_{3.0}$-40%O_2 were analyzed using X-ray photoelectron spectroscopy (XPS). As shown in Fig. S2, XPS survey spectra confirm the presence of C, N, and O elements in all samples, while Na is detected only in Na/O-$CN_{3.0}$ and Na/O-$CN_{3.0}$-40%O_2 samples. To further investigate the chemical bonds, high-resolution XPS spectra for C1s, N1s, O1s, and Na1s were presented in Fig. 4. In C1s XPS spectra (Fig. 4(a)), three distinct peaks are observed at 284.6, 286.0, and 288.0 eV, corresponding to C–C/C=C bonds, C–NH_x species in CN, and sp²-bonded carbon (N–C=N), respectively[32, 39, 42, 54]. N1s XPS spectra (Fig. 4(b)) show two common peaks across all samples at 398.4 and 401.0 eV, associated with sp² hybridized C=N–C in the triazine ring and amino groups (C–N–H), respectively[55]. Notably, the nitrogen-related peak at 399.9 eV shifts to a lower binding energy in Na/O-$CN_{3.0}$ sample, indicating slight disruption of N–$(C)_3$ moieties structure[39, 43]. The C–O bond and Na element are detected only in Na/O-$CN_{3.0}$ and Na/O-$CN_{3.0}$-40%O_2 samples (Fig. 4(c, d)), confirming the successful incorporation of Na and O atoms into these samples. In summary, the chemical bonds in Na/O-$CN_{3.0}$ are adjusted by doping Na and O atoms.

Additionally, electron spin resonance (ESR) measurement (Fig. S3) was conducted to analyze the defect structures. All samples exhibit the same Lorentzian line centered around a *g*-factor of 2.004, corresponding to unpaired electrons from sp² carbon atoms in the aromatic rings[11, 13, 15]. However, the peak intensities for Na/O-$CN_{3.0}$ and Na/O-$CN_{3.0}$-40%O_2 are higher than those for pure CN, which is attributed to defects introduced by Na and O doping in Na/O-CN_x samples[56].

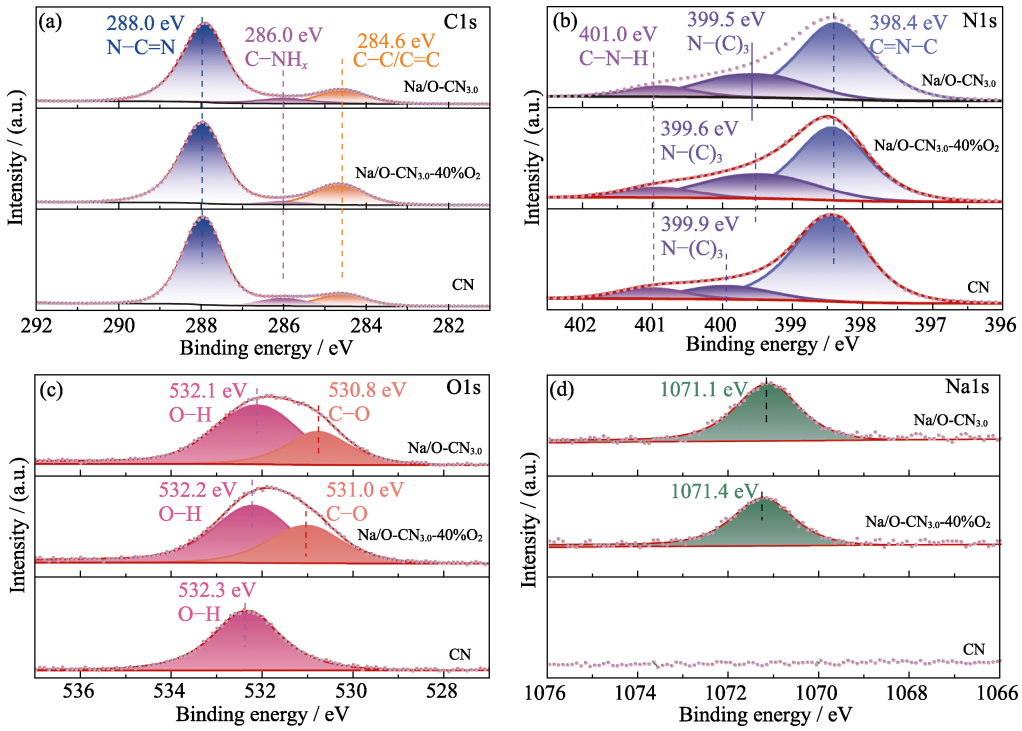

Fig. 4　High-resolution XPS spectra of pure CN, Na/O-$CN_{3.0}$ and Na/O-$CN_{3.0}$-40%O_2 samples
(a) C1s; (b) N1s; (c) O1s; (d) Na1s

2.2 Optical performance

To elucidate the impact of doping defects, the band structures of prepared samples were characterized using ultraviolet-visible diffuse reflectance spectroscopy (UV-Vis DRS), as shown in Fig. 5(a). Na/O-$CN_{3.0}$ exhibits a stronger absorption intensity compared to pure CN, which enhances the generation of photogenerated electron-hole pairs. The bandgap of Na/O-$CN_{3.0}$ is calculated to be 2.68 eV using the Tauc equation[57] (Fig. 5(b)), which is slightly lower than that of pure CN (2.70 eV). This reduction in bandgap improves its visible light absorption. To further investigate the band structures, valence band (VB) XPS spectra of the samples were measured (Fig. 5(c)). The VB values for pure CN and Na/O-$CN_{3.0}$ are determined to be 1.97 and 2.01 eV, respectively. The potential band structures are depicted in Fig. 5(d). The conduction band (CB) position of Na/O-$CN_{3.0}$ is slightly lower than that of pure CN but remains higher than the hydrogen reduction potential (H^+/H_2, 0 eV), making it suitable for water splitting applications[58].

Photocurrent and electrochemical impedance spectroscopy (EIS) measurements (Fig. 6(a, b)) were conducted to analyze the photocarrier separation and transfer capabilities. Na/O-$CN_{3.0}$ displays a higher photocurrent density compared to pure CN, indicating enhanced formation of photogenerated electron-hole pairs. Similarly, Na/O-$CN_{3.0}$ exhibits a smaller arc radius in the Nyquist plot than pure CN, reflecting improved conductivity. Additionally, photoluminescence (PL) tests of Na/O-$CN_{3.0}$ and pure CN, presented in Fig. 6(c, d), reveal that the PL intensity of Na/O-$CN_{3.0}$ is lower than that of pure CN, suggesting a reduced recombination rate of photogenerated electron-hole pairs in Na/O-$CN_{3.0}$ compared to pure CN[52]. The fluorescence lifetime of Na/O-$CN_{3.0}$ is 1.26 ns, slightly shorter than pure CN (1.38 ns), as shown in Fig. 6(d), corresponding to more efficient charge separation and transfer capabilities[59]. Therefore, doping Na and O atoms in Na/O-$CN_{3.0}$ improves photocarrier separation and electron transfer, and enhances its photocatalytic hydrogen evolution.

2.3 Photocatalytic hydrogen activity

The photocatalytic hydrogen evolution performances of prepared samples are shown in Fig. 7. As depicted in Fig. 7(a), all Na/O-CN_x samples exhibit an increased photocatalytic hydrogen evolution rate (PHER). The PHER of Na/O-CN_x samples initially rises with the increasing content of sodium citrate, but decreases when x exceeds 3.0. These results indicate that suitable co-doping with Na and O atoms is beneficial for the photocatalytic activity of Na/O-CN_x samples.

To further explore the synergistic effects between Na and O atoms, PHER of Na/O-$CN_{3.0}$-yO_2 samples synthesized under varying oxygen contents were analyzed (Fig. 7(b)). Na/O-$CN_{3.0}$-$0O_2$ sample shows higher photocatalytic hydrogen evolution than pure CN, indicating that Na doping is a key factor in improving photocatalytic activity. As oxygen content increases,

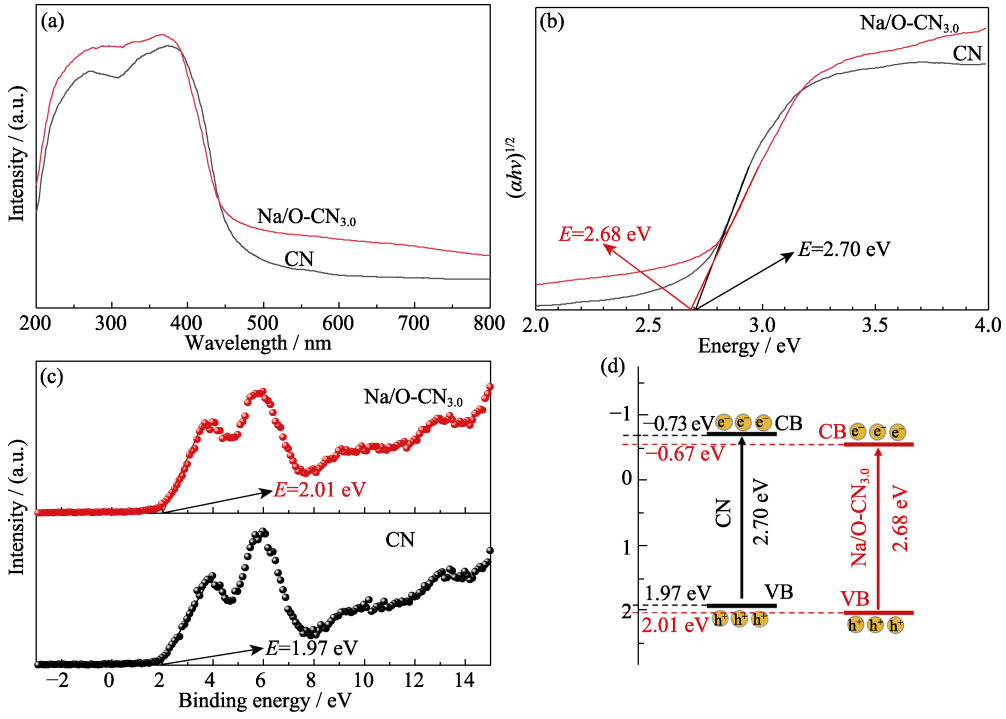

Fig. 5 Band structure analysis of pure CN and Na/O-$CN_{3.0}$

(a) UV-Vis DRS spectra; (b) Related Tauc plots; (c) VB XPS spectra; (d) Band structure diagram

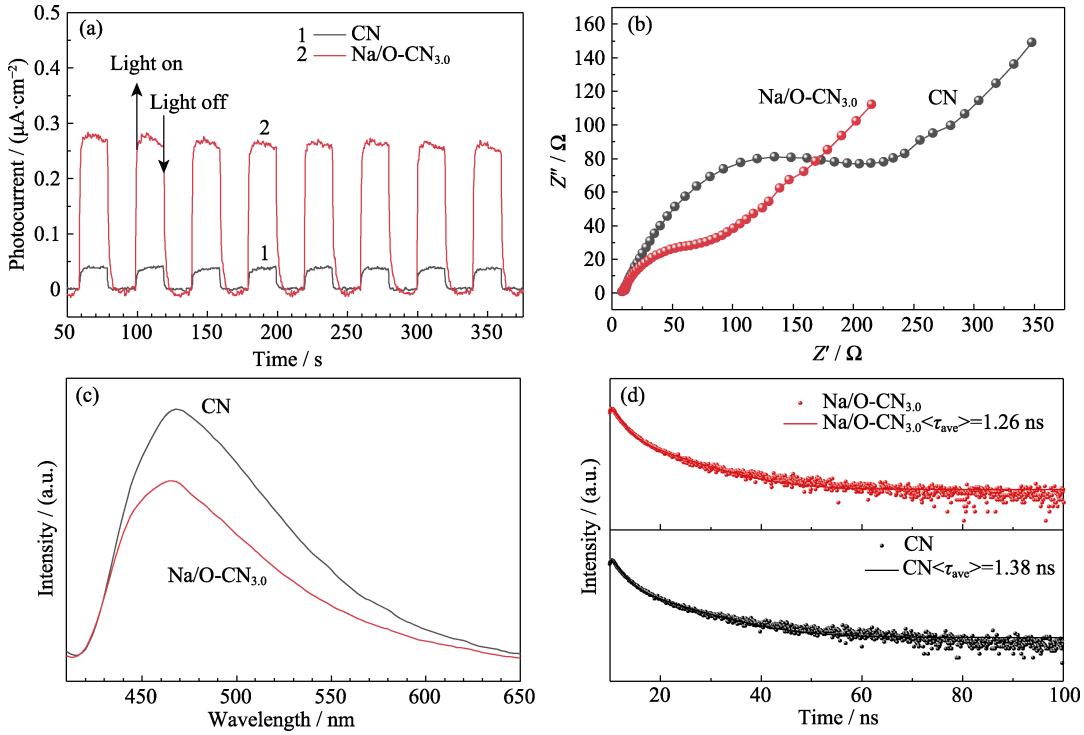

Fig. 6　Photocurrent and PL spectra analysis of pure CN and Na/O-$CN_{3.0}$ samples
(a) Photocurrent test; (b) EIS plots; (c) PL spectra; (d) Time-resolved PL spectra

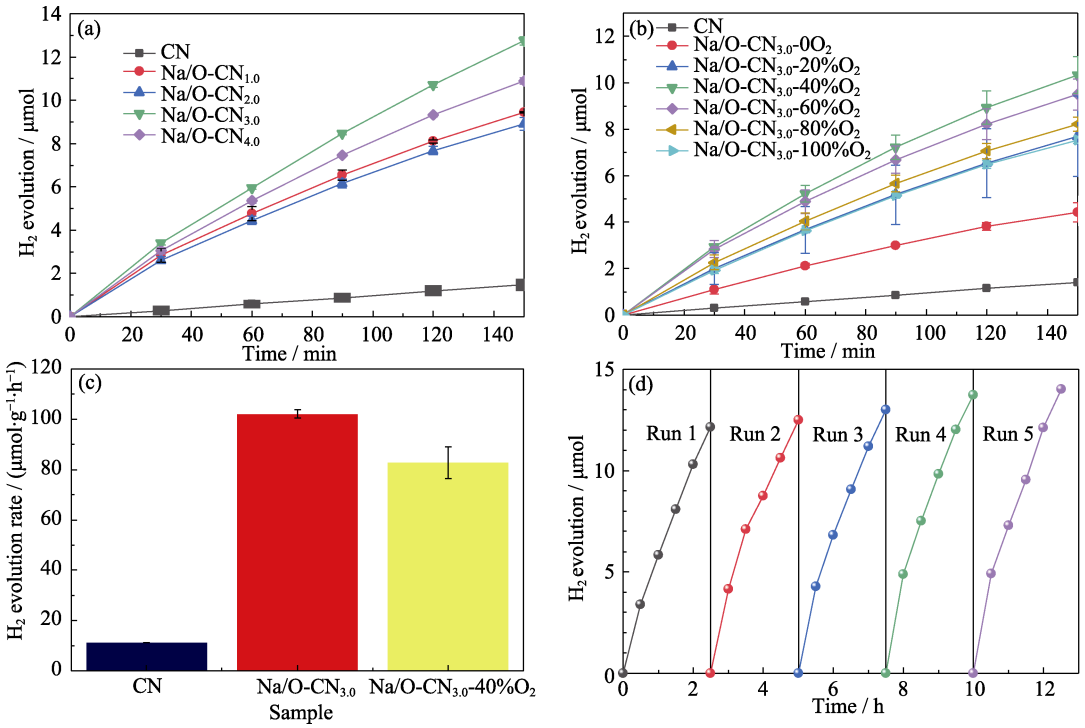

Fig. 7　Photocatalytic hydrogen activity
(a, b) Photocatalytic hydrogen evolution of (a) pure CN and Na/O-CN_x, and (b) Na/O-$CN_{3.0}$-yO_2;
(c) PHER of pure CN, Na/O-$CN_{3.0}$ and Na/O-$CN_{3.0}$-40%O_2; (d) Cycling performance of Na/O-$CN_{3.0}$

PHER of Na/O-$CN_{3.0}$-yO_2 first rises, then decreases when oxygen content exceeds 40%, demonstrating that suitable O doping also positively impacts photocatalytic activity. Therefore, the enhanced photocatalytic activity of Na/O-CN_x samples is attributed to the synergistic effect of Na and O atom doping. Among the samples, Na/O-$CN_{3.0}$ shows the highest photocatalytic hydrogen evolution, with a PHER of 103.2 μmol·g^{-1}·h^{-1} (Fig. 7(c)), which is 8.2 times higher than that of pure CN (11.2 μmol·g^{-1}·h^{-1}). Additionally, Na/O-$CN_{3.0}$ stands out

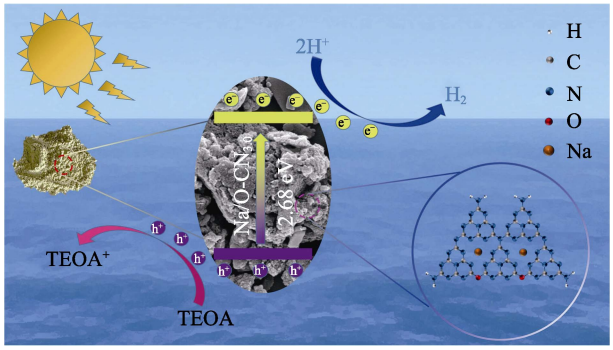

Fig. 8 Photocatalytic hydrogen evolution mechanism of Na/O-$CN_{3.0}$ under visible light irradiation

as a strong photocatalyst for hydrogen evolution, compared to other reported alkali metal-doped carbon nitride samples, as shown in Table S1. Interestingly, PHER of Na/O-$CN_{3.0}$ synthesized under air (with approximately 21% O_2) surpasses those of all Na/O-$CN_{3.0}$-yO_2 samples, likely due to the presence of some unknown trace gases in the air.

Then Na/O-$CN_{3.0}$ was chosen for the stability test. As shown in Fig. 7(d), PHER of Na/O-$CN_{3.0}$ remains stable over a 12.5 h cycling experiment. After the first cycle, PHER of Na/O-$CN_{3.0}$ slightly increases, which may be due to *in-situ* formation of co-catalyst Pt during the photocatalytic reaction.

2.4 Photocatalytic mechanism

Based on the discussions above, the proposed photocatalytic hydrogen evolution mechanism for Na/O-$CN_{3.0}$ is illustrated in Fig. 8. Under visible light irradiation, Na/O-$CN_{3.0}$ is excited to generate photogenerated electrons, which combine with H^+ ions to produce hydrogen gas. Simultaneously, the corresponding holes are involved in the oxidation of triethanolamine (TEOA). Due to the synergistic effect of Na and O atom doping, Na/O-$CN_{3.0}$ exhibits enhanced production of photogenerated electron-hole pairs while reducing their recombination rate. Consequently, Na/O-$CN_{3.0}$ demonstrates significantly higher photocatalytic hydrogen evolution activity compared to pure CN.

3 Conclusions

In summary, Na/O-CN_x were synthesized using NaCA as the sodium source at relatively low temperature. Na/O-CN_x samples exhibit an increased surface area, providing more active sites for reactions. The improved structure facilitates the transfer of photogenerated charges and enhances their production. Consequently, Na/O-CN_x samples achieve significantly higher photocatalytic hydrogen evolution rates compared to pure CN while maintaining excellent stability. This study offers a novel strategy for synthesizing alkali metal-doped carbon nitride at lower temperature, enabling highly efficient photocatalytic hydrogen evolution.

Supporting Materials

Supporting materials related to this article can be found at https://doi.org/10.15541/jim20240345.

References:

[1] SU C W, PANG L D, QIN M, *et al*. The spillover effects among fossil fuel, renewables and carbon markets: evidence under the dual dilemma of climate change and energy crises. *Energy*, 2023, **274:** 127304.

[2] LI Y M, ALHARTHI M, AHMAD I, *et al*. Nexus between renewable energy, natural resources and carbon emissions under the shadow of transboundary trade relationship from South East Asian economies. *Energy Strategy Rev.*, 2022, **41:** 100855.

[3] PANG L D, ZHU M N, YU H Y, *et al*. Is green finance really a blessing for green technology and carbon efficiency? *Energy Econ.*, 2022, **114:** 106272.

[4] INDRAWIRAWAN S, SUN H Q, DUAN X G, *et al*. Nanocarbons in different structural dimensions (0–3D) for phenol adsorption and metal-free catalytic oxidation. *Appl. Catal. B Environ.*, 2015, **179:** 352.

[5] LIN Y Y, HUNG K Y, LIU F Y, *et al*. Photocatalysts of quaternary composite, bismuth oxyfluoride/bismuth oxyiodide/graphitic carbon nitride: synthesis, characterization, and photocatalytic activity. *Mol. Catal.*, 2022, **528:** 112463.

[6] ZHANG Z, YANG L, LIU J R, *et al*. Improved oxygen electrocatalysis at FeN_4 and CoN_4 sites *via* construction of axial coordination. *Chin. Chem. Lett.*, 2025, **36(2):** 110013.

[7] XU T, DING X T, CHENG H H, *et al*. Moisture-enabled electricity from hygroscopic materials: a new type of clean energy. *Adv. Mater.*, 2023, **36(12):** 2209661.

[8] MANDAL D, ANDRADA D M. Oil droplets cut to the chase. *Nat. Chem.*, 2020, **12(12):** 1089.

[9] NISHIYAMA H, YAMADA T, NAKABAYASHI M, *et al*. Photocatalytic solar hydrogen production from water on a 100-m^2 scale. *Nature*, 2021, **598(7880):** 304.

[10] TANG D, TAN G L, LI G W, *et al*. State-of-the-art hydrogen generation techniques and storage methods: a critical review. *J. Energy Storage*, 2023, **64:** 107196.

[11] LI C Q, DU X, JIANG S, *et al*. Constructing direct Z-scheme heterostructure by enwrapping $ZnIn_2S_4$ on CdS hollow cube for efficient photocatalytic H_2 generation. *Adv. Sci.*, 2022, **9(24):** 2201773.

[12] HISATOMI T, DOMEN K. Reaction systems for solar hydrogen production *via* water splitting with particulate semiconductor photocatalysts. *Nat. Catal.*, 2019, **2(5):** 387.

[13] YI S S, ZHANG B X, WULAN B R, *et al*. Non-noble metals applied to solar water splitting. *Energy Environ. Sci.*, 2016, **9(11):** 145.

[14] JIAO Y Y, LI Y K, WANG J S, *et al*. Exfoliation-induced exposure of active sites for g-C_3N_4/N-doped carbon dots heterojunction to improve hydrogen evolution activity. *Mol. Catal.*, 2020, **497:** 111223.

[15] CHU X Y, LUAN B B, HUANG A X, *et al*. Controlled synthesis of 2D–2D conductive metal–organic framework/g-C_3N_4 heterojunctions for efficient photocatalytic hydrogen evolution. *Dalton Trans.*, 2024, **53(6):** 2534.

[16] YANG Y, ZHOU C Y, WANG W J, *et al*. Recent advances in application of transition metal phosphides for photocatalytic

hydrogen production. *Chem. Eng. J.*, 2021, **405:** 126547.

[17] SONG B, CHEN M, ZENG G M, *et al*. Using graphdiyne (GDY) as a catalyst support for enhanced performance in organic pollutant degradation and hydrogen production: a review. *J. Hazard. Mater.*, 2020, **398:** 122957.

[18] XIANG Q J, YU J G, JARONIEC M. Synergetic effect of MoS_2 and graphene as cocatalysts for enhanced photocatalytic H_2 production activity of TiO_2 nanoparticles. *J. Am. Chem. Soc*., 2012, **134(15):** 6575.

[19] XIAO S N, DAI W R, LIU X Y, *et al*. Microwave-induced metal dissolution synthesis of core–shell copper nanowires/ZnS for visible light photocatalytic H_2 evolution. *Adv. Energy Mater.*, 2019, **9(22):** 1900775.

[20] LI H H, WU Y, LI L, *et al*. Adjustable photocatalytic ability of monolayer g-C_3N_4 utilizing single–metal atom: density functional theory. *Appl. Surf. Sci.*, 2018, **457:** 735.

[21] SHANG Y Y, MA Y J, CHEN X, *et al*. Effect of sodium doping on the structure and enhanced photocatalytic hydrogen evolution performance of graphitic carbon nitride. *Mol. Catal.*, 2017, **433:** 128.

[22] YE Z W, YUE W H, TAYYAB M, *et al*. Simple one-pot, high-yield synthesis of 2D graphitic carbon nitride nanosheets for photocatalytic hydrogen production. *Dalton Trans.*, 2022, **51(48):** 18542.

[23] SHI J Y, ZHANG J, CUI Z W, *et al*. *In situ* growth of MOF-derived sulfur vacancy-rich CdS nanoparticles on 2D polymers for highly efficient photocatalytic hydrogen generation. *Dalton Trans.*, 2022, **51(15):** 5841.

[24] HUANG X, WU K Y, SU C, *et al*. Metal-organic framework Cu-BTC for overall water splitting: a density functional theory study. *Chin. Chem. Lett.*, 2025, **36(4):** 109720.

[25] WANG X C, MAEDA K, THOMAS A, *et al*. A metal-free polymeric photocatalyst for hydrogen production from water under visible light. *Nat. Mater.*, 2009, **8(1):** 76.

[26] YI S S, YAN J M, WULAN B R, *et al*. Noble-metal-free cobalt phosphide modified carbon nitride: an efficient photocatalyst for hydrogen generation. *Appl. Catal. B Environ.*, 2017, **200:** 477.

[27] HE J J, SUN H Q, INDRAWIRAWAN S, *et al*. Novel polyoxometalate@g-C_3N_4 hybrid photocatalysts for degradation of dyes and phenolics. *J. Colloid Interface Sci.*, 2015, **456:** 15.

[28] LI H H, WU Y, LI C, *et al*. Design of Pt/t-ZrO_2/g-C_3N_4 efficient photocatalyst for the hydrogen evolution reaction. *Appl. Catal. B Environ.*, 2019, **251:** 305.

[29] ZHOU A Q, YANG J M, ZHU X W, *et al*. Self-assembly construction of NiCo LDH/ultrathin g-C_3N_4 nanosheets photocatalyst for enhanced CO_2 reduction and charge separation mechanism study. *Rare Met.*, 2022, **41(6):** 2118.

[30] ZHU X W, XU H M, BI C Z, *et al*. Piezo-photocatalysis for efficient charge separation to promote CO_2 photoreduction in nanoclusters. *Ultrason. Sonochem.*, 2023, **101:** 106653.

[31] WU M, YAN J M, TANG X N, *et al*. Synthesis of potassium-modified graphitic carbon nitride with high photocatalytic activity for hydrogen evolution. *ChemSusChem*, 2014, **7(9):** 2654.

[32] ZHU Y L, SUN Y Y, KHAN J, *et al*. NaClO-induced sodium-doped cyano-rich graphitic carbon nitride nanosheets with nitrogen vacancies to boost photocatalytic hydrogen peroxide production. *Chem. Eng. J.*, 2022, **443:** 136501.

[33] ZHAO X L, ZHANG Y G, LI F, *et al*. Salt-air template synthesis of Na and O doped porous graphitic carbon nitride nanorods with exceptional photocatalytic H_2 evolution activity. *Carbon*, 2021, **179:** 42.

[34] HAN X, KANG Y, SONG S, *et al*. Sodium ion doped graphitic carbon nitride with high crystallinity for superior photocatalytic hydrogen evolution efficiency. *J. Mater. Chem. A*, 2023, **11(34):** 18213.

[35] DOU Q, HOU J H, HUSSAIN A, *et al*. One-pot synthesis of sodium-doped willow-shaped graphitic carbon nitride for improved photocatalytic activity under visible-light irradiation. *J. Colloid Interface Sci.*, 2022, **624:** 79.

[36] SUN Z Z, TAN Y Y, SHI X K, *et al*. General method to introduce π-electrons into oxygen-doped porous carbon nitride for photocatalytic hydrogen evolution and toluene oxidation. *ACS Sustainable Chem. Eng.*, 2024, **12(2):** 1051.

[37] WANG Y X, WANG H, CHEN F Y, *et al*. Facile synthesis of oxygen doped carbon nitride hollow microsphere for photocatalysis. *Appl. Catal. B Environ.*, 2018, **231:** 43.

[38] REN J X, ZHENG Y M, LIN H W, *et al*. Near-infrared light-activated g-C_3N_4 with effective n → π* electron transition for H_2O_2 production. *Appl. Surf. Sci.*, 2023, **638:** 158053.

[39] WU M, HE X, JING B H, *et al*. Novel carbon and defects co-modified g-C_3N_4 for highly efficient photocatalytic degradation of bisphenol A under visible light. *J. Hazard. Mater.*, 2020, **384:** 121323.

[40] LI Y H, HO W K, LV K L, *et al*. Carbon vacancy-induced enhancement of the visible light-driven photocatalytic oxidation of NO over g-C_3N_4 nanosheets. *Appl. Surf. Sci.*, 2018, **430:** 380.

[41] LU X J, WANG Y, ZHANG X Y, *et al*. NiS and MoS_2 nanosheet co-modified graphitic C_3N_4 ternary heterostructure for high efficient visible light photodegradation of antibiotic. *J. Hazard. Mater.*, 2018, **341:** 10.

[42] HU S Y, YU A C, LU R. A comparison study of sodium ion- and potassium ion-modified graphitic carbon nitride for photocatalytic hydrogen evolution. *RSC Adv.*, 2021, **11(26):** 15701.

[43] FANG W J, LIU J Y, YU L, *et al*. Novel (Na, O) co-doped g-C_3N_4 with simultaneously enhanced absorption and narrowed bandgap for highly efficient hydrogen evolution. *Appl. Catal. B Environ.*, 2017, **209:** 631.

[44] MA R D, GUO X, SHI K X, *et al*. S-type heterojunction of MOS_2/g-C_3N_4: construction and photocatalysis. *J. Inorg. Mater.*, 2023, **38(10):** 1176.

[45] CHEN X, LI H K, WU Y X, *et al*. Facile fabrication of novel porous graphitic carbon nitride/copper sulfide nanocomposites with enhanced visible light driven photocatalytic performance. *J. Colloid Interface Sci.*, 2016, **476:** 132.

[46] KRÖGER J, JIMÉNEZ‐SOLANO A, SAVASCI G, *et al*. Interfacial engineering for improved photocatalysis in a charge storing 2D carbon nitride: melamine functionalized poly(heptazine imide). *Adv. Energy Mater.*, 2021, **11(6):** 2003016.

[47] LIU M Q, JIAO Y Y, QIN J C, *et al*. Boron doped C_3N_4 nanodots/nonmetal element (S, P, F, Br) doped C_3N_4 nanosheets heterojunction with synergistic effect to boost the photocatalytic hydrogen production performance. *Appl. Surf. Sci.*, 2021, **541:** 148558.

[48] YANG C W, XUE Z, QIN J Q, *et al*. Heterogeneous structural defects to prompt charge shuttle in g-C_3N_4 plane for boosting visible-light photocatalytic activity. *Appl. Catal. B Environ.*, 2019, **259:** 118094.

[49] SHI L, LIU G, ZHANG Y H, *et al*. Na, O co-doping and cyano groups synergistically adjust the band structure of g-C_3N_4 for improving photocatalytic oxygen evolution. *Mater. Res. Bull.*, 2023, **167:** 112423.

[50] GU J, CHEN H, JIANG F, *et al*. Visible light photocatalytic mineralization of bisphenol A by carbon and oxygen dual-doped graphitic carbon nitride. *J. Colloid Interface Sci.*, 2019, **540:** 97.

[51] IQBAL O, ALI H, LI N, *et al*. A review on the synthesis, properties, and characterizations of graphitic carbon nitride (g-C_3N_4) for energy conversion and storage applications. *Mater. Today Phys.*, 2023, **34:** 101080.

[52] OU H H, LIN L H, ZHENG Y, *et al*. Tri-*s*-triazine-based

crystalline carbon nitride nanosheets for an improved hydrogen evolution. *Adv. Mater.*, 2017, **29(22):** 1700008.
[53] ZHOU J, YANG Y, ZHANG C Y. A low-temperature solid-phase method to synthesize highly fluorescent carbon nitride dots with tunable emission. *Chem. Commun.*, 2013, **49(77):** 8605.
[54] ZHANG Y Z, ZONG S C, CHENG C, *et al*. One-pot annealing preparation of Na-doped graphitic carbon nitride from melamine and organometallic sodium salt for enhanced photocatalytic H_2 evolution. *Int. J. Hydrog. Energy*, 2018, **43(30):** 13953.
[55] GUO F, CHEN J L, ZHANG M W, *et al*. Deprotonation of g-C_3N_4 with Na ions for efficient nonsacrificial water splitting under visible light. *J. Mater. Chem. A*, 2016, **4(28):** 10806.
[56] WU M, CHEN L B, LUO X, *et al*. Defective carbon nitride with dual-surface engineering for highly efficient photocatalytic hydrogen evolution under visible light irradiation. *Langmuir*, 2024, **40(34):** 18153.
[57] MAKUŁA P, PACIA M, MACYK W. How to correctly determine the band gap energy of modified semiconductor photocatalysts based on UV–Vis spectra. *J. Phys. Chem. Lett.*, 2018, **9(23):** 6814.
[58] YU H J, SHI R, ZHAO Y X, *et al*. Alkali-assisted synthesis of nitrogen deficient graphitic carbon nitride with tunable band structures for efficient visible-light-driven hydrogen evolution. *Adv. Mater*., 2017, **29(26):** 1605148.
[59] WULANA B R, YI S S, LI S J, *et al*. Amorphous nickel pyrophosphate modified graphitic carbon nitride: an efficient photocatalyst for hydrogen generation from water splitting. *Appl. Catal. B Environ.*, 2018, **231:** 43.

Na 和 O 元素共掺杂氮化碳高效光催化制氢

陈莉波[1], 盛 盈[1], 伍 明[1], 宋季岭[2], 蹇 建[1], 宋二红[3]

(1. 湖南科技大学 化学化工学院, 湘潭 411201; 2. 国家复合改性聚合物工程技术研究中心, 贵阳 550014; 3. 中国科学院 上海硅酸盐研究所, 上海 200050)

摘 要: 元素掺杂可以调控氮化碳(CN)能带结构以获取更好的光催化性能。本研究通过柠檬酸钠和纯 CN 粉末的固相反应, 在 180 ℃空气气氛下制备了 Na 和 O 共掺杂 CN(Na/O-CN_x, x=1.0、2.0、3.0、4.0)。Na/O-$CN_{3.0}$ 的比表面积达到 18.8 m^2/g, 比纯 CN(11.7 m^2/g)提升了 60.7%。Na/O-$CN_{3.0}$ 样品的能带宽度为 2.68 eV, 略低于纯 CN(2.70 eV), 前者有助于可见光吸收。Na 和 O 元素共掺杂有效抑制了材料的光生电子-空穴对复合, 提升了太阳光的利用率。因此, Na/O-CN_x 样品在可见光条件下的光催化制氢效率得到了显著提升, 最优催化剂 Na/O-$CN_{3.0}$ 的光催化制氢效率为 103.2 μmol·g^{-1}·h^{-1}, 相比于纯 CN(11.2 μmol·g^{-1}·h^{-1})提升了 8.2 倍, 同时表现出良好的催化稳定性。此外, 通过调节反应气体中氧含量制备了一系列 Na/O-$CN_{3.0}$-$y$$O_2$($y$=0、20%、40%、60%、80%、100%)样品, 催化性能结果揭示了在 Na/O-CN_x 样品中掺杂 Na 和 O 原子均有助于提升光催化性能。本工作为较低温度下制备金属原子掺杂 CN 材料提供了新思路, 揭示了 Na 和 O 原子在 Na/O-CN_x 光催化制氢过程中的协同效应。

关 键 词: Na 和 O 共掺杂氮化碳; 协同效应; 可见光; 光催化制氢

中图分类号: TQ174 **文献标志码:** A **文章编号:** 1000-324X(2025)05-0552-09

Supporting Materials:

Na and O Co-doped Carbon Nitride for Efficient Photocatalytic Hydrogen Evolution

CHEN Libo[1], SHENG Ying[1], WU Ming[1], SONG Jiling[2], JIAN Jian[1], SONG Erhong[3]

(1. School of Chemistry and Chemical Engineering, Hunan University of Science and Technology, Xiangtan 411201, China;
2. National Engineering Research Center for Compounding and Modification of Polymer Materials, Guiyang 550014, China;
3. Shanghai Institute of Ceramics, Chinese Academy of Sciences, Shanghai 200050, China)

Photocatalytic hydrogen evolution test

Photocatalytic reactions of samples were conducted on an on-line photocatalytic hydrogen evolution system (CEL-PAEM-D8). 50 mg samples were dispersed in triethanolamine solution (50 mL, 10%, in volume) with 0.5 mL H_2PtCl_6 aqueous solution (1 mg/mL, Pt basis) as Pt source. Pt-CN and Pt-Na/O-CN_x samples were synthesized with *in situ* photo-deposition method by 30 min simulated sunlight irradiation. Photocatalytic hydrogen reaction was operated under vacuum condition with visible light irradiation of a 300 W xenon-lamp (CEL-HXF 300) equipped with a 420 nm cutoff filter (AULIGHT). Reaction solution temperature was kept below 6 ℃ with a flow of cooling water, and obtained hydrogen was analyzed by gas chromatography (GC7920-TFZA).

Catalyst characterization

Powder X-ray diffraction (XRD) patterns were performed on a Bruker D8 Advance X-ray diffractometer with Cu Kα irradiation (λ=1.5406 Å) by a scan rate of 5 (°)/min. Transmission electron microscope (TEM) images were acquired using the JEOL JEM-F200. Scanning electron microscope (SEM) images were obtained utilizing the ZEISS Sigma 300. X-ray photoelectron spectroscopy (XPS) was measured using the Thermo Scientific K-Alpha spectrometer, with the C1s reference peak positioned at 284.6 eV. The Shimadzu UV-3600 spectrophotometer was employed to acquire the ultraviolet-visible diffuse reflectance spectrum (UV-Vis DRS) of prepared samples. The fluorescence lifetime and photoluminescence (PL) spectra of the sample were measured on the FLS1000 transient fluorescence spectrometer. Fourier transform infrared (FT-IR) spectra were acquired using the Thermo Scientific iN10 instrument. The Micromeritics ASAP 2460 analyzer was utilized to determine the Brunauer-Emmett-Teller (BET) surface areas through N_2 adsorption. Electron spin resonance (ESR) spectra of samples were recorded on JEOL JES-FA200 ESR spectrometer.

The electrochemical measurements were performed in a conventional three-electrode cell on a CHI-760E electrochemical workstation (Shanghai Chenhua Instrument Co., Ltd., China). During the photocurrent measurement, a saturated calomel electrode (SCE) was used as the reference electrode and a Pt foil electrode acted as the counter electrode. The working electrodes were designed using resulting samples covered on the surface of fluoride tin oxide (FTO) conductor glass. A quartz cell filled with 0.5 mol·L^{-1} Na_2SO_4 electrolyte was used as the measuring system. For electrochemical impedance spectroscopy (EIS) measurements, the amplitude of the sinusoidal wave was 5 mV, and the frequency range was from 100 kHz to 0.1 Hz.

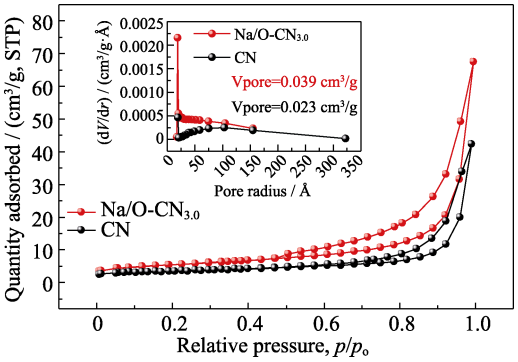

Fig. S1　Nitrogen adsorption-desorption isotherms and corresponding pore diameter distribution curves of pure CN and Na/O-$CN_{3.0}$

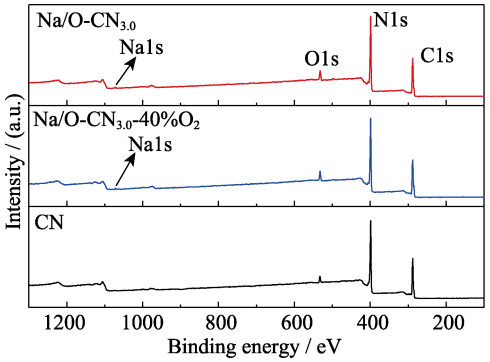

Fig. S2　XPS survey spectra of pure CN, Na/O-$CN_{3.0}$ and Na/O-$CN_{3.0}$-40%O_2

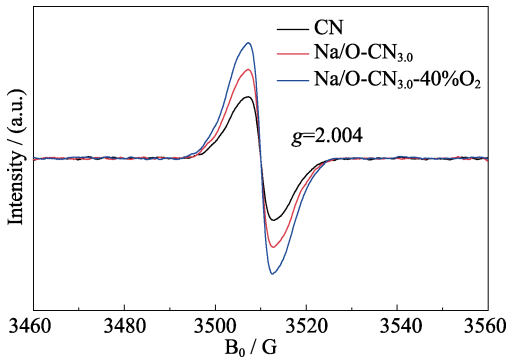

Fig. S3 ESR spectra of pure CN, Na/O-$CN_{3.0}$ and Na/O-$CN_{3.0}$-40%O_2 samples

Table S1 Photocatalytic hydrogen evolution performance under visible light irradiation (> 420 nm) and surface area of alkali metal doped carbon nitride[S1-S12]

Catalyst	Synthesis temperature/℃	Catalyst weight/mg	Sacrificial reagent/% (in volume)	Surface area/ ($m^2 \cdot g^{-1}$)	Activity compared with CN (times)	Ref.
Na/O-$CN_{3.0}$	180	50	TEOA 10%	18.8	9.2	This work
3% NaCl-CN	550	10	TEOA 17%	76.8	4.3	[S1]
KCN-10	550	50	TEOA 10%	11	5.6	[S2]
K(0.05)-CN	550	50	TEOA 17%	11.1	5	[S3]
LiNa-K-CN2	520	50	TEOA 10%	116.2	15	[S4]
Na(30)-MCN	550	100	TEOA 10%	56.1	12.9	[S5]
Na0.1-CNNTs	650	20	TEOA 10%	94	11	[S6]
CN-Na-7	550	50	TEOA 10%	11.7	9.9	[S7]
CN-100	520	50	TEOA 10%	14.9	9.2	[S8]
(Na,O)g-C_3N_4	160	50	ethyl alcohol 40%	–	7	[S9]
$CN_{0.05}$	550	20	TEOA	46.7	1.9	[S10]
GCN-Na-5	550	50	TEOA	10.3	1.5	[S11]
K@C_3N_4	600	100	TEOA	27.5	8	[S12]

References:

[S1] CHEN Y, WANG X C. Template-free synthesis of hollow G-C_3N_4 polymer with vesicle structure for enhanced photocatalytic water splitting. *J. Phys. Chem. C*, 2018, **122(7):** 3786.

[S2] WANG Y Y, ZHAO S, ZHANG Y W, *et al.* One-pot synthesis of K-doped g-C_3N_4 nanosheets with enhanced photocatalytic hydrogen production under visible-light irradiation. *Appl. Surf. Sci.*, 2018, **440:** 258.

[S3] CHANG X Y, FAN H Q, ZHU S W, *et al.* Engineering doping and defect in graphitic carbon nitride by one-pot method for enhanced photocatalytic hydrogen evolution. *Ceram. Int.*, 2023, **49(4):** 6729.

[S4] BAI P, WANG P, LI T, *et al.* Alkali functionalized carbon nitride with internal van der Waals heterostructures: directional charge flow to enhance photocatalytic hydrogen production. *J. Colloid Interface Sci.*, 2023, **644:** 211.

[S5] SHU Z, WANG Y, WANG W B, *et al.* A green one-pot approach for mesoporous g-C_3N_4 nanosheets with *in situ* sodium doping for enhanced photocatalytic hydrogen evolution. *Int. J. Hydrog. Energy*, 2019, **44(2):** 748.

[S6] ZHANG L S, DING N, HASHIMOTO M, *et al*. Sodium-doped carbon nitride nanotubes for efficient visible light-driven hydrogen production. *Nano Res.*, 2018, **11(4):** 2295.

[S7] SHANG Y Y, MA Y J, CHEN X, *et al.* Effect of sodium doping on the structure and enhanced photocatalytic hydrogen evolution performance of graphitic carbon nitride. *Mol. Catal.*, 2017, **433:** 128.

[S8] ZHANG Y Z, ZONG S C, CHENG C, *et al.* One-pot annealing preparation of Na-doped graphitic carbon nitride from melamine and organometallic sodium salt for enhanced photocatalytic H_2 evolution. *Int. J. Hydrog. Energy*, 2018, **43(30):** 13953.

[S9] FANG W J, LIU J Y, YU L, *et al.* Novel (Na, O) co-doped g-C_3N_4 with simultaneously enhanced absorption and narrowed bandgap for highly efficient hydrogen evolution. *Appl. Catal. B Environ.*, 2017, **209:** 631.

[S10] DOU Q, HOU J H, HUSSAIN A, *et al.* One-pot synthesis of sodium-doped willow-shaped graphitic carbon nitride for improved photocatalytic activity under visible-light irradiation. *J. Colloid Interface Sci.*, 2022, **624:** 79.

[S11] HU S Y, YU A C, LU R, A comparison study of sodium ion- and potassium ion-modified graphitic carbon nitride for photocatalytic hydrogen evolution. *RSC Adv.*, 2021, **11(26):** 15701.

[S12] ZHANG G Q, ZHU J Y, XU Y S, *et al.* In-plane charge transport dominates the overall charge separation and photocatalytic activity in crystalline carbon nitride. *ACS Catal.*, 2022, **12(8):** 4648.